Chapter 5.4 – Long range surface plasmon-enhanced fluorescence spectroscopy as a platform for biosensors

Amal Kasry, Jakub Dostálek and Wolfgang Knoll*
Max Planck Institute for Polymer Research, Ackermannweg 10, 55128 Mainz, Germany
** Current Address: Cardiff School of Biosciences, Museum Avenue, Cardiff, CF10 3US, UK*

Abstract
Long range surface plasmons (LRSPs) are electromagnetic waves originating from the coupling between two surface plasmons propagating on opposite interfaces of a thin metal layer surrounded by dielectrics with similar refractive indices. These electromagnetic waves can propagate along the metal film with an order of magnitude lower damping compared to conventional surface plasmons. Therefore, the excitation of LRSPs is associated with a high enhancement of field intensity at the metal–dielectric interface. In surface plasmon enhanced fluorescence spectroscopy (SPFS), this feature increases the fluorescence signal enabling a more precise observation of binding processes of biomolecules in the proximity to the metal surface. In this chapter, we demonstrate recent advancements in LRSP-enhanced fluorescence spectroscopy and its implementation in SPFS-based biosensors.

5.4.1 Introduction

Over the last two decades, great strides have been achieved in the development of biosensors for fast and sensitive detection of numerous compounds relevant to important areas such as environmental monitoring, food control and medical diagnostics[1-3]. Optical biosensors based on surface plasmon resonance (SPR) are devices which exploit surface plasmon (SP) waves excited at a metallic surface[4]. These surface waves probe the interactions between target molecules present in a liquid sample and biomolecular recognition elements anchored to the metallic surface. The capture of target molecules on the metallic surface causes an increase in the refractive index which can be observed using the spectroscopy of SPs. This label-free approach enables the direct detection of large and medium size molecules (typically >10kDa) which can produce sufficiently high refractive index changes. In order to increase the sensitivity of the measurement of the binding of target molecules, surface plasmon-enhanced fluorescence spectroscopy (SPFS) was introduced to SPR biosensors[5]. SPFS-based biosensors take advantage of the increased intensity of the electromagnetic field on the metallic surface occurring upon the excitation of SPs. The SP field is used to excite the chromophore-labeled molecules bound to the surface providing thus large enhancement of the fluorescence signal. In comparison with SPR biosensors relying on the measurement of refractive index changes, SPFS-based biosensors typically enable detection of analytes with several orders of magnitude lower detection limits[6].

With the advent of SPR biosensors, various surface plasmon modes were employed for the refractive index and fluorescence spectroscopy-based observation of biomolecular binding events. These include long range surface plasmons (LRSP)[7], SPs coupled to a dielectric waveguide[8], Bragg-scattered SPs[9] and localized SPs supported by metallic nanoparticles[10] and nano-structured metallic surfaces[11]. LRSP is a special surface plasmon mode which originates from the coupling of surface plasmons (SPs) propagating along opposite surfaces of a thin metal film. LRSPs can propagate with an order of magnitude lower damping compared to conventional SPs[12]. Therefore, LRSPs have attracted attention for the design of high-resolution SPR sensors[13, 14] and currently an ultra-high refractive index resolution (smallest detectable RI change) of 2.5×10^{-8} was reported[15]. Only recently, LRSPs were applied in SPFS-based biosensors[16, 17]. Due to their low damping, the excitation of LRSPs is associated with a large enhancement of field intensity at the metal–dielectric interface which can be directly translated into an increase in the fluorescence signal.

Within this chapter, we describe recent advancements in SPFS-based biosensors achieved through the excitation of LRSPs. In the following, we describe the characteristics of LRSPs, the arrangements used for their excitation and their implementation in a biosensor. A comparison of the performance of SPFS-based biosensors relying on the excitation of conventional SPs and LRSPs is presented.

5.4.2 Surface plasmon modes propagating on a thin metal film

A surface plasmon (SP) is an optical wave trapped on a metallic surface which originates from coupled collective oscillations of the electron plasma and the associated electromagnetic field, see Fig. 1a. This optical wave propagates along an interface between a semi-infinite metal and a dielectric medium with the complex propagation constant β:

$$\beta = k_0 \sqrt{\frac{n_m^2 n_d^2}{n_m^2 + n_d^2}}, \tag{1}$$

where $k_0=2\pi/\lambda$ is the wave vector of light in vacuum, λ is the wavelength, n_d is the refractive index of the dielectric and n_m is the (complex) refractive index of the metal. The optical field of SP is transverse magnetic (TM) and by using the Cartesian coordinates shown in Fig. 1a it is described by the following nonzero components: magnetic intensity parallel to the interface H_y, electric intensity parallel to the interface E_z and electric intensity perpendicular to the interface E_x. The SP field exponentially decays from the metal – dielectric interface with the penetration depth $L_{pen}=(\beta^2-k_0^2n^2)^{-1/2}$ where n is equal to n_m for the metal and n_d for the dielectric. The penetration depth is defined as the distance perpendicular to the surface at which the field amplitude decreases by a factor 1/e. The energy of SP dissipates while it propagates along the metal surface due to the losses within the metal film. This damping can be described by the propagation length $L_{pro}=(2\mathrm{Im}\{\beta\})^{-1}$ as the distance along the metallic surface at which the intensity of the SP mode drops to 1/e.

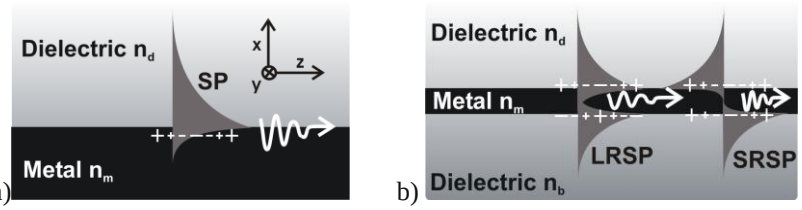

a) b)

Fig. 1a) Surface plasmon propagating on a metal-dielectric interface, b) symmetrical (LRSP) and anti-symmetrical (SRSP) surface plasmon modes coupled though a thin metal film embedded in a dielectric.

In order to illustrate typical characteristics of SPs, let us assume a wavelength in the visible part of the spectrum λ=0.633 μm and the interface between a gold with the refractive index of n_m=0.1 + 3.5i and a dielectric with n_d=1.33. For these parameters, the field distribution of SP is depicted in Fig. 2. The penetration depth of SP into the dielectric is equal to L_{pen}=0.183 μm and that into the gold is L_{pen} =0.027 μm. The propagation length of the SP reaches L_{pro}=7.2 μm.

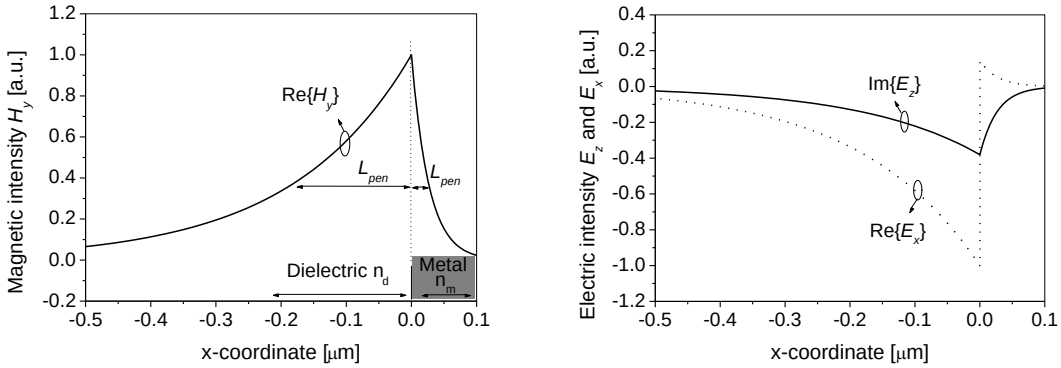

a) **b)**

Fig. 2 Distribution of a) the magnetic intensity *Hy* and b) the electric intensities E_x and E_z of SP propagating along the interface of gold (n_m=0.1 + 3.5) and a dielectric (n_d=1.33); wavelength of λ=0.633 μm.

Further, let us investigate SP modes propagating along a thin metal film embedded between two dielectrics with refractive indices of n_d and n_b, see Fig. 1b. In general, this geometry with two metallic interfaces supports two SP modes with propagation constants that obey the following equation:

$$\tan\left(\frac{\kappa d_m}{2}\right) = \frac{\gamma_d n_m^2/\kappa n_d^2 + \gamma_b n_m^2/\kappa n_b^2}{1-\left(\gamma_d n_m^2/\kappa n_d^2\right)\left(\gamma_b n_m^2/\kappa n_b^2\right)}, \tag{2}$$

where d_m is the thickness of the metal film, $\kappa^2=(k_0^2 n_m^2-\beta^2)$ and $\gamma^2_{d,b}=\beta^2-k_0^2 n^2_{d,b}$.

If the refractive indices of the dielectrics are identical n_d=n_b, SPs on the two metallic interfaces can couple giving rise to two new SP modes. Owing to the symmetry of the configuration, these two modes exhibit symmetrical and anti-symmetrical distribution of the magnetic intensity H_y. By solving the equation (2), there can be shown that Re{β} of the symmetrical mode is smaller than that of a regular SP on an individual interface and it decreases upon decreasing the metal slab thickness d_m. On the contrary, Re{β} of the anti-symmetrical mode is larger than that of a regular SP and it increases when decreasing the thickness d_m, see Fig. 3a. The propagation length L_{pro} of the symmetrical mode is larger and that of anti-symmetrical mode is smaller than the one of SP, see Fig. 3b. Therefore, the symmetrical and anti-symmetrical modes are referred to as long range surface plasmon (LRSP) and short-range surface plasmon (SRSP), respectively. For thicknesses of the metallic film which are much larger than the penetration depth of SP into the metal d_m>>L_{pen}, the coupling across the metal film disappears and thus the propagation constant β of LRSP and SRSP approaches that for the SP on a single metal – dielectric interface. For small thicknesses d_m, SPs on opposite interfaces are coupled strongly and the LRSP propagation constant approaches the one of light in the dielectric with refractive index n_d=n_b and the propagation constant of SRSP diverges.

For instance, on a gold film with the thickness of d_m=20 nm and a refractive index of n_m=0.1+3.5i, dielectrics with n_d=n_b=1.33 and a wavelength of λ=0.633 μm, the propagation length of LRSP and SRSP reaches L_{pro}=190 μm and 0.78 μm, respectively. If the geometry in not exactly symmetrical n_d<>n_b, there exist a thickness of the metal film d_m below which the LRSP mode cease to exist. This thickness is referred to as cut-off thickness: for example, at a wavelength of λ=0.633 μm and a gold film embedded in dielectrics with n_b=1.333 and n_d=1.340 it is equal to d_m=8 nm.

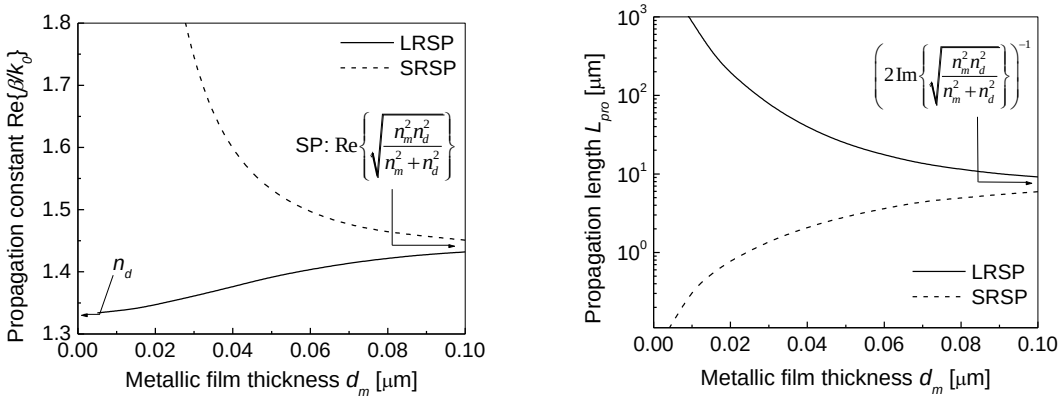

a) **b)**

Fig. 3 a) The real part of the propagation constant and b) the propagation length L_{pro} for LRSP and SRSP on a gold film with d_m= 0-0.1 μm, n_m=0.1+3.5i, n_d=n_b=1.33 and λ=0.633 μm.

The electromagnetic fields of both LRSP and SRSP exponentially decay into the dielectrics and exhibit the maximum intensity at the metal film interfaces. As seen in Fig. 4, the LRSP mode exhibits a symmetrical distribution of H_y and E_x and an anti-symmetrical profile for E_z. Complementary to that, the SRSP mode has an anti-symmetrical profile of H_y and E_x and a symmetrical profile of the E_z. In general, SP modes are strongest coupled to the oscillations of electron plasma density through the component E_z. Because this component for LRSP is anti-symmetrical across the metallic film (see Fig. 4a), this mode is weakly coupled to the electron plasma oscillations and thus its damping is lowered and the penetration depth into the dielectrics L_{pen} is enlarged. Contrary to this, the E_z distribution of SRSP is symmetrical (see Fig. 4b) leading to a stronger coupling with the electron plasma oscillations and, hence, an increased damping and lowered penetration depth L_{pen}.

The electromagnetic field distribution of LRSP and SRSP presented in Fig. 4 was calculated for a gold film with a thickness of d_m=20 nm, dielectrics with refractive indices of n_b=n_d=1.33 and a wavelength of λ=0.633 μm. For such a structure, the penetration depth of the LRSP into the dielectric is of L_{pen}=556 nm and that of SRSP is of L_{pen}=65 nm.

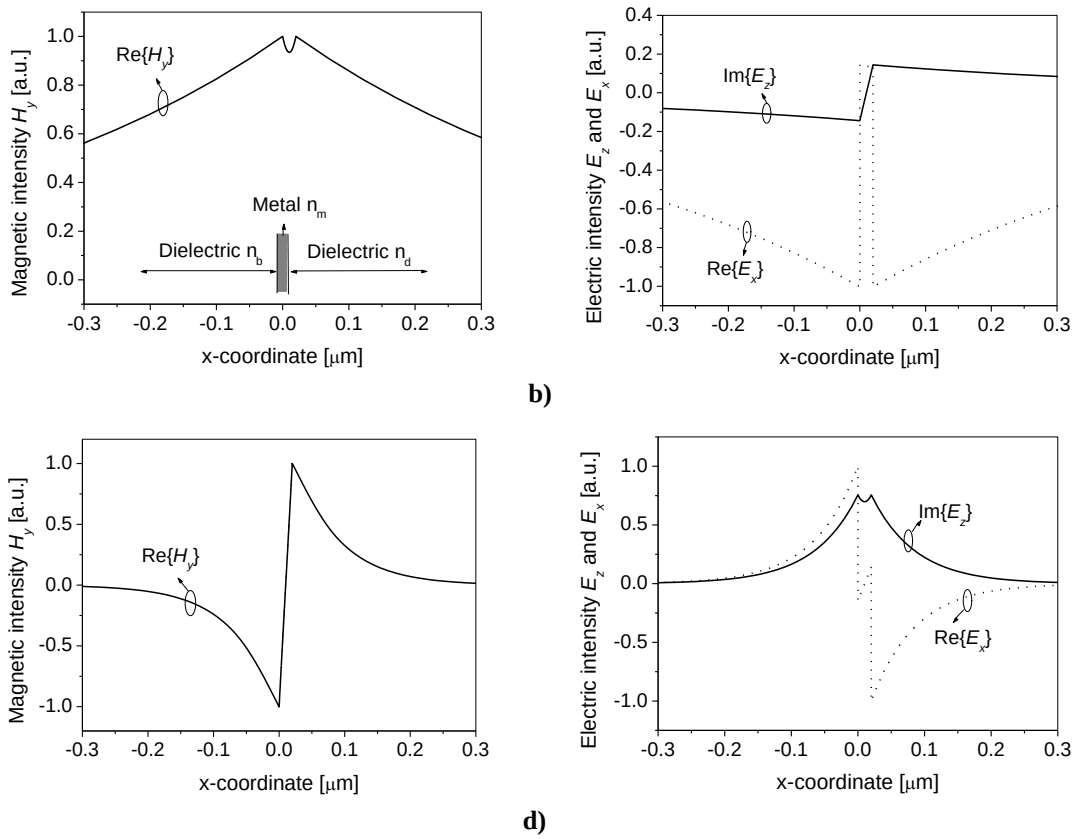

Fig. 4 Components of the electromagnetic field components H_y, E_x and E_z calculated for a,b) a LRSP and c,d) a SRSP mode, d_m=20 nm, n_m=0.1+3.5i, n_d=n_b=1.33 and λ=633 nm.

5.4.3 Optical excitation of LRSPs

In order to efficiently couple light to a LRSP, the photon and LRSP waves need to be phase matched along the metallic surface. As the Re{β} of LRSP is always larger than the wave vector of a light wave in the dielectric $k_0 n_{b,d}$, a prism coupler[12, 13] can be used to enhance the momentum of the incident light and thus enable an efficient transfer of energy to LRSP.

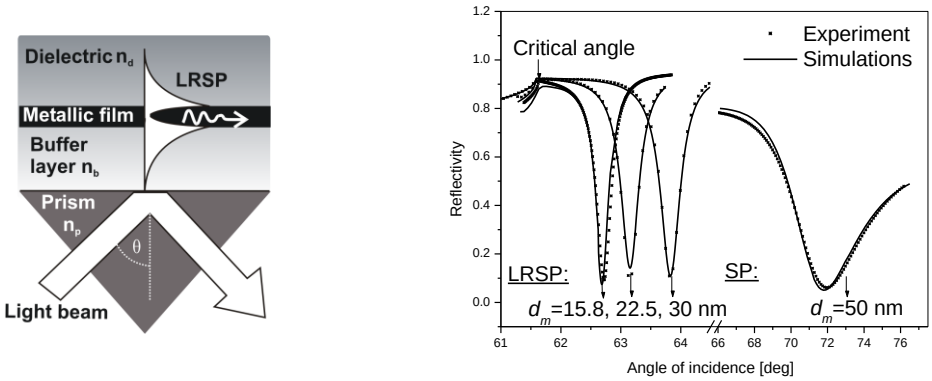

Fig. 5 a) Scheme of a prism coupler for the excitation of LRSPs; b) Comparison of the angular reflectivity spectra measured for the excitation of SP and LRSPs using a BK7 prism (n_p=1.515), a Cytop buffer layer (n_b=1.340, d_b=900 nm), a gold film (d_m indicated in the graph and n_m=0.18+3.1i for d_m=22.5 nm), water as a dielectric medium (n_d=1.333) and a light beam with a wavelength of λ=633 nm, reproduced from [17].

In the prism coupler, a light beam is launched into a prism with a refractive index n_p which is higher than that of the buffer layer n_b and the top dielectric n_d (Fig. 5a). Upon the incidence of the light beam at the interface between the prism and buffer layer, the light beam is totally reflected and coupled through its evanescent tail to LRSP if the following phase-matching condition is fulfilled:

$$k_0 n_p \sin(\theta) = \mathrm{Re}\{\beta\}. \tag{3}$$

As illustrated in the angular reflectivity spectrum in Fig. 5b, the excitation of LRSPs is manifested as a resonant dip centered at the angle of incidence for which equation (3) holds. The strength of the coupling between the optical wave and LRSP can be tuned by varying the thickness of the buffer layer d_b in order to achieve the full coupling of light to LRSPs. For example, for a gold film thickness of d_m=22.5 nm, buffer layer with n_b=1.340, a dielectric with n_b=1.333 and a wavelength of λ=633 nm, this optimum buffer layer thickness is close to d_b=900nm, see Fig. 5b.

The comparison of the reflectivity spectra measured for the excitation of LRSPs and a regular SP in Fig. 5b reveals that LRSPs are excited at lower angles of incidence than SP due to their lower real part of the propagation constant Re{β} (see Fig. 3a). In addition, the width of the resonant dip associated with the excitation of LRSP is more than an order of magnitude lower that that for SP due to the larger propagation length of LRSP (see Fig. 3b). For instance, the full width in half minima (FWHM) of the LRSP resonance on a gold film with d_m=22.5 nm is $\Delta\theta$=0.4 deg compared to $\Delta\theta$=5.1 deg for the excitation of a regular SP.

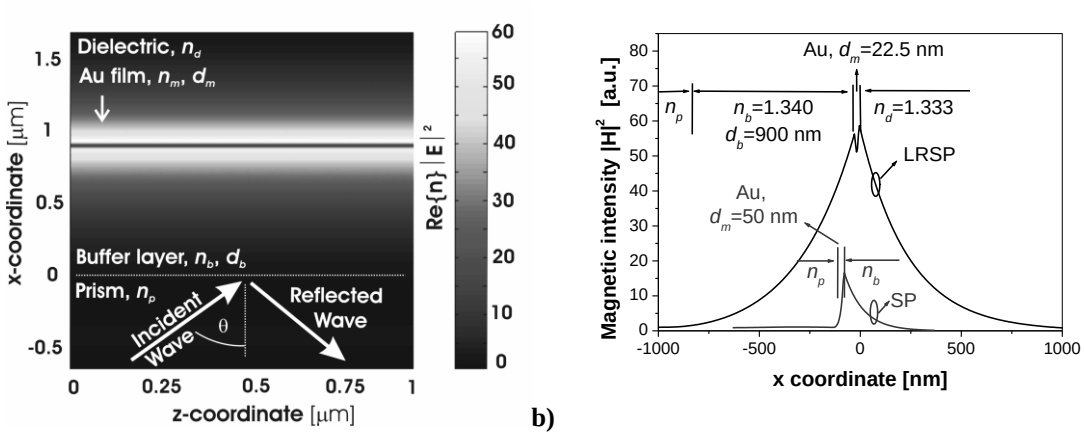

Fig. 6 a) Simulations of the electric intensity distribution of LRSPs excited on a gold film with d_m=22.5 nm (electric intensity of the incident plane wave is equal to 1). b) Comparison of the magnetic intensity profile for the excitation of LRSP and conventional SP. The same parameters as in Fig.5b were used and the light wave was incident on the prim base at an angle of incidence of θ=63.1 deg.

Upon the excitation of LRSP, the energy carried by the incident wave is accumulated within the LRSP leading to the enhancement of the field intensity in the vicinity of the metallic film. In general, the magnitude of the field intensity enhancement is increasing with the propagation length L_{pro}. In Fig. 6a, the distribution of the electric intensity field is presented for a LRSP excited on a 22.5 nm thick with a plane wave incident at the resonant angle of θ=63.1 deg (parameters of the layer structure: n_p=1.515, d_b=900 nm, n_b=1.340, n_m=0.18+3.1i and n_d=1.333, wavelength of λ=633 nm). For such a geometry, the electric intensity $|E_x|^2 + |E_z|^2$ on the top of the gold surface is 60 times larger than that of the incident wave. For comparison, the field intensity enhancement achieved through the excitation of SPs on a gold film at the same wavelength is 16 [17]. In addition, the field intensity enhancement is achieved within larger region adjacent to the metallic film due to the higher penetration depth of LRSP, see Fig. 6b.

5.4.4 Implementation of LRSPs in a SPFS based biosensor

In SPFS-based biosensors, LRSPs are used for the excitation of chromophore-labeled molecules captured by biorecognition elements anchored on a metallic sensor surface. These devices incorporate two key components: i) an optical structure providing the enhancement of the electromagnetic field through the excitation of LRSPs and ii) detection assay and the binding matrix with immobilized ligands for the capture of target molecules.

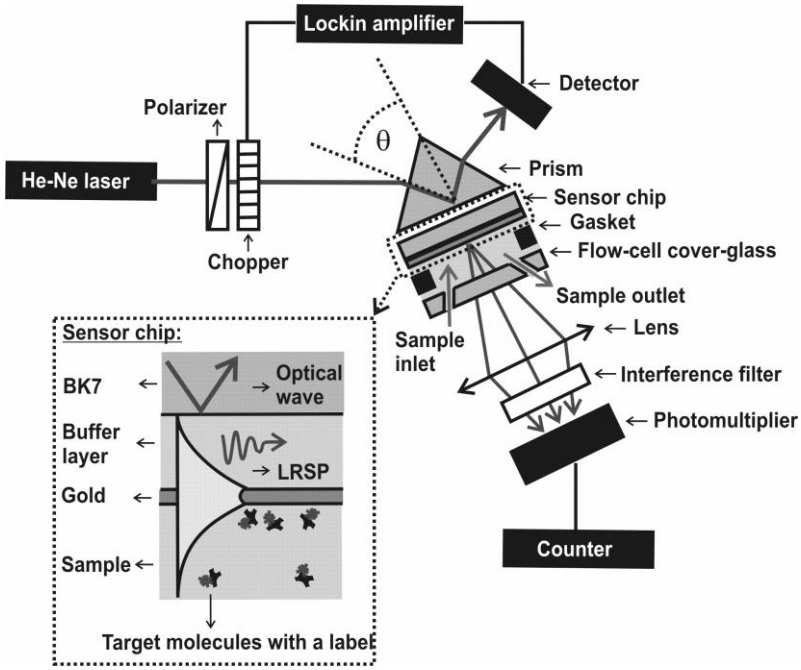

Fig. 7 Optical setup of a sensor based on the spectroscopy of LRSPs for the detection of biomolecular binding events on a metallic surface using the label-free detection principle and LRSP-enhanced fluorescence spectroscopy; reproduced from [17].

In the LRSP-enhanced fluorescence spectroscopy, mostly prism couplers utilizing the attenuated total internal reflection method (ATR) were used [16, 17], see Fig. 7. A monochromatic light beam with the wavelength matching the absorption band of a chromophore is coupled to a high refractive index prism. On the base of the prism, a sensor chip with a layer coating supporting LRSPs is optically matched. The sensor chip consists of a glass slide, a low refractive index buffer layer and a thin metal film. For biosensor applications, on the top of the metal film an additional layer with biorecognition elements capable to capture target molecules from aqueous samples is prepared. Against the sensor chip, a transparent flow-cell with the analyte solution is attached. The fluorescence light is detected using a lens optics, a band-pass filter to suppress the background due to the scattered light at the excitation wavelength and a photomultiplier or CCD-based detector.

In order to achieve a refractive index symmetrical structure needed for the excitation of LRSPs, the refractive index of the buffer layer n_b needs to match to that of aqueous samples which is close to that of water n_d=1.333 (at λ=633 nm). Up to date, different commercially available Teflon-based materials [13, 14] (Teflon AF from Dupont Inc., USA, with n_b=1.31 and Cytop from Asahi Inc., Japan, with n_b=1.34), low refractive index dielectrics such as aluminum fluoride (AlF_3, n_b=1.34) [18] or magnesium fluoride (MgF_2, n_b=1.38) [14] and nanoporous silicates (the refractive index can be tuned by the size of pores) were used. These materials can be spincoated (Teflon) or deposited by vacuum thermal evaporation (magnesium and aluminum fluoride). For the excitation of surface plasmons in the visible and NIR part of the spectrum, noble metals are employed. Among these, gold is preferably used owing to its stability. Gold films are mostly prepared by sputtering or vacuum thermal evaporation. As shown before [17], gold films with thicknesses smaller than d_m~20 nm exhibit an island morphology if deposited by these techniques on surfaces with low surface energy such as Teflon. This effect leads to the deteriorating of their optical properties

In LRSP-enhanced fluorescence spectroscopy, various surface chemistries developed for SPR or SPFS biosensors can be used [19]. For LRSP-based sensors, particularly three-dimensional binding matrices are of interest by which the whole extended evanescent field of LRSP can be used for the sensing. Currently, research in novel hydrogel-based materials which can used for the construction of three-dimensional binding matrices is carried out [20, 21].

5.4.5. Comparison of LRSP and SP-enhanced fluorescence spectroscopy

As illustrated in the previous sections 5.4.2 and 5.4.3, the excitation of LRSPs results in an enhancement of the intensity of the electromagnetic field at a metallic surface. If compared to conventional surface plasmons, the enhancement in close proximity to the gold surface by the factor of up to 4 was reported [17]. In addition, the evanescent field of LRSP can extend into the medium on top of the gold surface with up to order of magnitude higher depth. These features enables increasing the fluorescence signal due to the capture of chromophore-labeled molecules on the sensor surface as a larger number of molecules can be excited with a higher excitation rate.

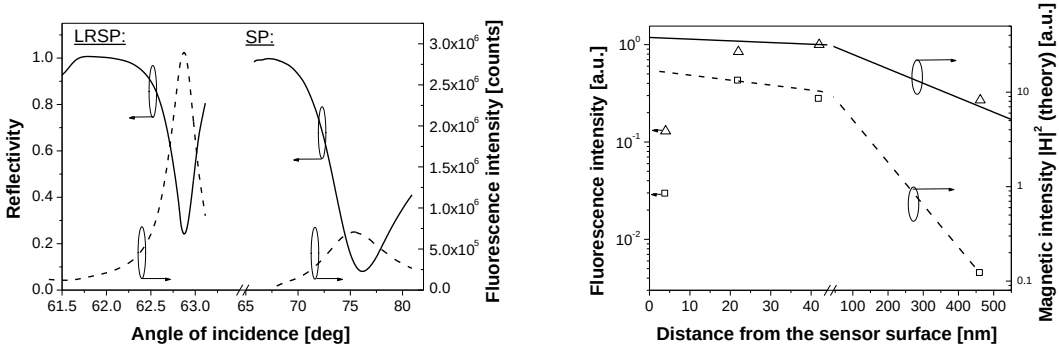

Fig. 8 Comparison of the fluorescence signal recorded via the excitation of LRSP and SP. a) Angular reflectivity and fluorescence intensity spectra measured for a monolayer of chromophore-labeled molecules deposited at a distance of 42 nm from the sensor surface. b) The dependence of the maximum fluorescence intensity on the distance of the chromophore from the sensor surface. Reproduced from [17].

Experimental results confirmed these predictions [16, 17]. Using a low refractive index spacer layers, a monolayer of chromophore-labeled molecules was bound at different distances from the gold sensor surface. The dependence of the fluorescence intensity on the distance was measured upon the excitation of chomophores via SP (on a 50 nm thick gold film) and via LRSP (propagating along a 16 nm thick gold film between a Cytop buffer layer and the aqueous sample). As seen in the measured reflectivity and fluorescence intensity spectra in Fig. 8a, the maximum fluorescence signal is detected during the resonat excitation of the surface plasmon modes. For the chromophore excitation by LRSPs, the fluorescence intensity is detected within a narrower range of angles of incidence and exhibits a higher peak intensity than found upon the excitation by conventional SPs. The comparison of the fluorescence signal in Fig. 8b reveals that the fluorescence intensity decays exponentially for the chromophore-labeled monolayer deposited at distances larger than 40 nm. For smaller distance, we observed a decrease in the peak fluorescence intensity due to the non-radiative decay of a dye induced by the presence of the metal [22]. Assuming the excitation of dyes distributed within the whole evanescent field of LRSP and SP, the overall enhancement in the collected fluorescence intensity can be assumed as the product of the enhancement in the proximity to the sensor surface (4.4 measured at a distance of 4 nm) and the ratio of the penetration depths (for LRSP with d_{Au}=15.8 nm and conventional SP this ratio is equal to 2.9). By this means, we can estimate that more than an order of magnitude increase in the fluorescence intensity can be achieved by taking advantage of the higher enhancement and the more extended field of LRSP when compared with conventional SPS.

5.4.5. LRSP-enhanced fluorescence spectroscopy: biomolecular binding studies

In SPFS-based biosensors, the binding of chromophore-labeled analyte molecules from a sample to their biomolecular partners on the sensor surface is measured through induced fluorescence signal. The biomolecular partners (biorecognition elements) can be immobilized on the sensor surface using various architectures [23] including monolayer assemblies or three-dimensional binding matrices. In general, a three-dimensional binding matrix attached to the sensor surface allows for a higher sensor response as whole evanescent field of a surface plasmon mode can be exploited. Within such a binding matrix, a higher amount of ligand molecules can be immobilized and thus stronger fluorescence signal can be observed. As was reported by Yu et al., a three-dimensional dextrane brush binding matrix (CM5 sensor chip from Biacore Inc., USA) loaded with a mouse immunoglobulin G (IgG) enabled the detection of anti-mouse IgG antibodies at a concentrations as low as 500 aM (80 fg/mL)[24] by using surface plasmon enhanced fluorescence spectroscopy. In this experiment, the dextrane brush with thickness of ~100 nm was used which matches the penetration depth of surface plasmon (see Fig. 2).

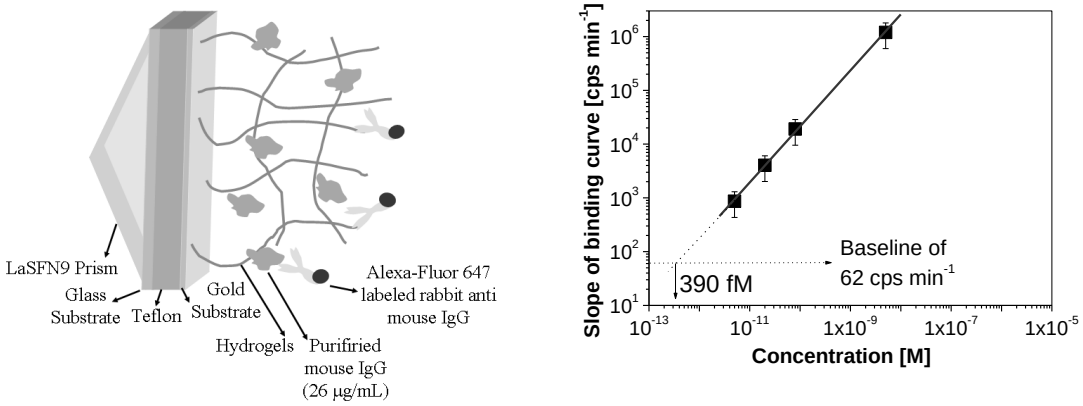

Fig. 9. a) A scheme of the LRSPR sample with the hydrogel matrix indicating the protein binding to the matrix. b) the calibration curve of the sensor measured for the binding of anti-mouse IgG to mouse IgG anchored within the hydrogel binding matrix.

In order to let SPFS benefit from LRSP which exhibits a more extended evanescent field (see Fig. 2 and Fig. 4), a three-dimensional binding matrix with up to micrometer thickness needs to be developed. A first attempt to achieve this goal was carried out using a NIPAAM [N-(isopropylacrylamide)]-based hydrogel[21] deposited on a LRSP-supporting layer structure (Teflon AF with thickness of d_b=500 and a gold film with a thickness d_{Au}=40 nm), see Fig9a. Briefly, carboxyl groups within the polymer were activated by incubating in a mixture of trifluoroacetyl-N-succinimidyl ester (TFA-NHS) in CH_2C_{l2} and $N(Et)_3$ for 24h under Ar at room temperature. Afterwards, the polymer was precipitated in Et_2O, spincoated on a gold surface which was modified with an adhesion promoter containing a thiol group (synthesized in the lab), crosslinked with UV light and swelled in phosphate buffer saline (PBS). The thickness and the refractive index of the swollen hydrogel were determined as 402 nm and 1.345, respectively. A purified mouse IgG (from Invitrogen, USA) was *in situ* covalently bound into the hydrogel from a solution with the concentration of mouse IgG of 20 μg/mL. After the immobilization of mouse IgG, the sensor surface was washed out with PBS. The refractive index of the hydrogel after the immobilization of mouse IgG was of 1.3463 which indicates the IgG surface coverage of 2.6 ng mm^{-2}.

Using such prepared hydrogel matrix, the binding of anti-mouse IgG (from Invitrogen Inc., USA) labeled with Alexa Fluor dye (Alexa Fluor 647 from Molecular Probes Inc., USA) was measured using LRSP-enhanced fluorescence spectroscopy. A light beam at the wavelength of 633 nm was coupled to a LRSP wave to probe the binding in the hydrogel matrix. LRSP wave excited the chromophore-labeled anti-mouse IgG molecules which were affinity captured within the binding matrix. The fluorescence signal was measured in time while series of samples with anti-mouse IgG dissolved at concentrations of (40 aM, 5 fM, 5pM, 20 pM, 80pM, and 5 nM) were successively injected. Each sample was flowed along the sensor

surface for 10 min and the increase in the fluorescence signal due to anti-mouse IgG capture was determined. For each concentration, slope of time evolution of the fluorescence signal due to the binding of target molecule was determined. Preliminary results presented in Fig9b revealed that the NIPAAM-based hydrogel is suitable for a construction of binding matrix and achieved limit of detection (LOD) was of 400 fM (60 pg/mL).

5.4.6 Conclusions and future outlook

We described recent advances in surface plasmon-enhanced fluorescent spectroscopy (SPFS) through the implementation of special surface plasmon modes - long range surface plasmons (LRSPs). The characteristics of LRSPs, their excitation and implementation in SPFS biosensors were discussed. We showed that the excitation of LRSPs allows for a dramatic enhancement of the intensity of electromagnetic field at the sensor surface which can be directly translated into an increase in the fluorescence signal. In addition, LRSPs enables probing the medium adjacent to the sensor surface with its extended evanescent field up to a micron in depth. This feature allows for the detection of the fluorescence signal from a larger sensing volume in which a higher amount of chromophore-labeled molecules can be captured. The presented data indicates that this approach holds potential to increase the fluorescence signal intensity by more than an order of magnitude compared to conventional SPFS. Future research will include improvements of LRSP-based optics to reach even larger enhancement of electromagnetic field and higher yield of detected fluorescence light. Furthermore, novel materials for three-dimensional binding matrices are under investigation to fully exploit the potential of LRSPs enhanced fluorescence spectroscopy for design of new ultra sensitive biosensors. In addition, the extended evanescent field of LRSPs can provide advantage for the detection of large analytes such as bacteria.

Acknowledgements

We would like to thank and appreciate the help of Cathrin Corten and Dirk Kuckling (Technische Universität, Dresden) for supplying us with the NIPAAM polymer, Robert Roskamp (MPIP) for helping in the chemistry of the polymer activation, Maria Gianneli (MPIP) for helping in the polymer characterization by FCS, and Fang Yu for the useful discussions. Support by the Deutsche Forschungsgemainschaft (Priority Program SPP 1259: “Intelligente Hydrogele”, KN 224/18-1) is greatly acknowledged. In addition, this publication was financially supported by the European Commission in the Communities 6th Framework Programme, Project TRACEBACK (FOOD-CT-036300), and Coordinated by Tecnoalimenti. It reflects the author's views and the Community is not liable for any use that may be made of the information contained in this publication.

References:

1 M. A. Gonzalez-Martinez, R. Puchades and A. Maquieira, (2007), Optical immunosensors for environmental monitoring: How far have we come?, Analytical and Bioanalytical Chemistry 387, 205-218.

2 A. Rasooly and K. E. Herold, (2006), Biosensors for the analysis of food- and waterborne pathogens and their toxins, Journal of Aoac International 89, 873-883.

3 T. Vo-Dinh and B. Cullum, (2000), Biosensors and biochips: advances in biological and medical diagnostics, Fresenius Journal of Analytical Chemistry 366, 540-551.

4 H. Rather (1983) Surface Plasmons on Smooth and Rough Surfaces and on Gratings, Springer Verlag, Berlin.

5 T. Liebermann and W. Knoll, (2000), Surface-plasmon field-enhanced fluorescence spectroscopy, Colloids and Surfaces a-Physicochemical and Engineering Aspects 171, 115-130.

6 D. A. Healy, C. J. Hayes, P. Leonard, L. McKenna and R. O'Kennedy, (2007), Biosensor developments: application to prostate-specific antigen detection, Trends in Biotechnology 25, 125-131.

7 K. Matsubara, S. Kawata and S. Minami, (1990), Multilayer System for a High-Precision Surface-Plasmon Resonance Sensor, Optics Letters 15, 75-77.

8 F. C. Chien and S. J. Chen, (2006), Direct determination of the refractive index and thickness of a biolayer based on coupled waveguide-surface plasmon resonance mode, Optics Letters 31, 187-189.

9 J. Dostalek, P. Adam, P. Kvasnicka, O. Telezhnikova and J. Homola, (2007), Spectroscopy of Bragg-scattered surface plasmons for characterization of thin biomolecular films, Optics Letters 32, 2903.

10 S. Lal, S. Link and N. J. Halas, (2007), Nano-optics from sensing to waveguiding, Nature photonics 1, 641-648.

11 C. Genet and T. W. Ebbesen, (2007), Light in tiny holes, Nature 445, 39-46.

12 D. Sarid, (1981), Long-Range Surface-Plasma Waves on Very Thin Metal-Films, Physical Review Letters 47, 1927-1930.
13 G. G. Nenninger, P. Tobiska, J. Homola and S. S. Yee, (2001), Long-range surface plasmons for high-resolution surface plasmon resonance sensors, Sensors and Actuators B-Chemical 74, 145-151.
14 A. W. Wark, H. J. Lee and R. M. Corn, (2005), Long-range surface plasmon resonance imaging for bioaffinity sensors, Analytical Chemistry 77, 3904-3907.
15 S. Slavik and J. Homola, (2007), Ultrahigh resolution long range surface plasmon-based sensor, Sensors and Actuators B-Chemical 123, 10-12.
16 A. Kasry and W. Knoll, (2006), Long range surface plasmon fluorescence spectroscopy, Applied Physics Letters 89, 101106.
17 J. Dostalek, A. Kasry and W. Knoll, (2007), Long range surface plasmons for observation of biomolecular binding events at metallic surfaces, Plasmonics 2, 97-106.
18 M. Vala, J. Dostalek and J. Homola, (2007), Diffraction Grating-Coupled Surface Plasmon Resonance Sensor Based on Spectroscopy of Long-Range and Short-Range Surface Plasmons, SPIE 6585, 658522-658521.
19 S. Löfås and A. McWhirter (2006) in J. Homola (Ed.), Surface Plasmon Resonance Based Sensors, Springer, pp. 117-151.
20 P. W. Beines, I. Klosterkamp, B. Menges, U. Jonas and W. Knoll, (2007), Responsive thin hydrogel layers from photo-cross-linkable poly(N-isopropylacrylamide) terpolymers, Langmuir 23, 2231-2238.
21 A. Giannelli, P. W. Beines, R. F. Roskamp, K. Koynov, G. Fytas and W. Knoll, (2007), Local and global dynamics of transient polymer networks and swollen gels anchored on solid surfaces, Journal of Physical Chemistry C 111, 13205-13211.
22 K. Vasilev, W. Knoll and M. Kreiter, (2004), Fluorescence intensities of chromophores in front of a thin metal film, Journal of Chemical Physics 120, 3439-3445.
23 W. Knoll, H. Park, E. K. Sinner, D. F. Yao and F. Yu, (2004), Supramolecular interfacial architectures for optical biosensing with surface plasmons, Surface Science 570, 30-42.
24 F. Yu, B. Persson, S. Lofas and W. Knoll, (2004), Attomolar sensitivity in bioassays based on surface plasmon fluorescence spectroscopy, Journal of the American Chemical Society 126, 8902-8903.